Italian Association of Aeronautics and Astronautics
XXV International Congress
9-12 September 2019 | Rome, Italy

COMPUTATIONAL METHODS COUPLING PERIDYNAMICS WITH CLASSICAL MECHANICS: OUT OF BALANCE FORCES IN OVERALL STRUCTURAL EQUILIBRIUM

M. Zaccariotto[1*], G. Ongaro[1], T. Ni [2] P. Seleson[3], U. Galvanetto[1]

[1] Department of Industrial Engineering, University of Padova, v. Venezia 1, Italy

[2] College of Civil and Transportation Engineering, Hohai University, 210098, Nanjing, China

[3] Computer Science and Mathematics Division, Oak Ridge National Laboratory, USA

* mirco.zaccariotto@unipd.it

ABSTRACT

The paper investigates an often-overlooked issue in the use of coupled computational techniques: the assessment of overall static equilibrium. The analysis is focused on a peridynamic and FEM coupling computational method recently proposed by the authors. The magnitude of the out-of-balance forces obtained in all the examples is a fraction of a per cent of the applied forces, but it cannot be considered as a numerical error. The paper shows that the main reason for the occurrence of the out-of-balance forces is the presence of a highly non-linear rate of change of displacements in the coupling zone of the models.

Keywords: Peridynamic, FEM-PD coupling, out-of-balance forces.

1 INTRODUCTION

Cracks and defects are an unavoidable presence in many structures in particular in aeronautical and aerospace applications. Consequently, safety and economic needs require the capability to predict damage and crack evolution by adequate numerical techniques. Computational methods based on Classical Continuum Mechanics (CCM) have not been naturally developed to simulate problems involving discontinuities in the displacement field. Therefore, CCM-based computational tools have to be equipped with ad hoc extensions to cope with crack propagation problems. At the beginning of this century a new non-local theory formulated with integral equations, named Peridynamics (PD) [1-2], was presented with the aim of including cracks as part of the solution. However, PD is not computationally efficient, due to the non-local nature of the approach and that is a limitation to its practical use. To solve this issue, we introduced a FEM-PD coupling technique [3] in order to use the PD approach only in the regions of the model where cracks can arise or interact. The current coupling method [3] satisfies the usual numerical tests, that is rigid body motion, uniform and linear strain cases, but an often-overlooked issue in the use of coupled computational methods, adopting different models of solid mechanics [4], is the verification of overall structural equilibrium.

We will illustrate the problem through simple structural examples, partially discretized with a PD method and partially with a classical mechanics FEM approach. In our examples, using the coupling method presented in [3], the magnitude of the out-of-balance forces is small, compared to that of the acting forces, but it cannot be assumed to be a numerical error. Our work will study how the variation of the main features of the coupled model can affect the magnitude of the out-of-balance forces.

The paper is organized as follows: section 2 gives an overview of PD and FEM-PD coupling method; section 3 presents the out-of-balance forces issue in overall equilibrium; section 4 shows the results of several examples and, finally, the discussion of section 5 concludes the paper.

2 OVERVIEW OF PERIDYNAMICS AND FEM-PD COUPLING METHOD

2.1 Peridynamics and its discretization

In a body (***B***) modelled by PD a material point with position vector **x** (in the following referred to as point **x**) is associated to an infinitesimal volume dV_x, and it interacts with all surrounding points within a neighbourhood $H(\mathbf{x})$. The equation of motion of point **x** is defined by the following integro-differential equation:

$$\rho(\boldsymbol{x})\ddot{\boldsymbol{u}}(\boldsymbol{x},t) = \int_{H(\boldsymbol{x})}(\underline{\boldsymbol{T}}[\boldsymbol{x},t]\langle\boldsymbol{x}'-\boldsymbol{x}\rangle - \underline{\boldsymbol{T}}[\boldsymbol{x}',t]\langle\boldsymbol{x}-\boldsymbol{x}'\rangle)dV_{\boldsymbol{x}'} + \boldsymbol{b}(\boldsymbol{x},t),\ \boldsymbol{x}'\in H(\boldsymbol{x}) \qquad (1)$$

where ρ is the mass density, **u** is the displacement field, **b** is the body density force, $\underline{\boldsymbol{T}}[\boldsymbol{x},t]\langle\boldsymbol{x}'-\boldsymbol{x}\rangle$ stands for the force vector state which indicates the force density vector that point $\mathbf{x}'$ exerts on point **x**, and the neighbourhood $H(\mathbf{x}):=\{\mathbf{x}'\in\Omega:\ |\mathbf{x}'-\mathbf{x}|\leq\delta\}$ is the integration region usually taken to be a sphere, in 3D, or a circle, in 2D, centred at **x** . The radius δ of $H(\mathbf{x})$ is called the horizon of **x**. The vector of relative position between two points $\boldsymbol{\xi}=\mathbf{x}'-\mathbf{x}$ is called bond. In OSB-PD [2], the material is taken to be homogenous and the force state $\underline{\boldsymbol{T}}$ depends only on the deformation state so that a force density vector is aligned with the corresponding deformed bond. In this way, the force density can be written as:

$$\underline{\boldsymbol{T}}[\boldsymbol{x},t]\langle\boldsymbol{x}'-\boldsymbol{x}\rangle = \underline{t}[\boldsymbol{x},t]\langle\boldsymbol{x}'-\boldsymbol{x}\rangle\bar{\boldsymbol{e}} \qquad (2)$$

where $\underline{t}$ is the modulus state the value of which depends on the constitutive law of the material. According to [2], $\underline{t}$ can be determined in terms of classical constants in the case of linear elastic solids [5,6] and $\bar{\boldsymbol{e}}$ is a unit vector aligned with the deformed bond. Bond Based -PD (BB-PD) [1] can be considered as a particular case of the OSB-PD. In fact, in BB-PD the interaction between two points is completely independent of other bonds, and the force density that point $\mathbf{x}'$ exerts on point **x** ($\underline{\boldsymbol{T}}[\boldsymbol{x},t]\langle\boldsymbol{x}'-\boldsymbol{x}\rangle$) and that point **x** exerts on point $\mathbf{x}'$ ($\underline{\boldsymbol{T}}[\boldsymbol{x}',t]\langle\boldsymbol{x}-\boldsymbol{x}'\rangle$) are equal in magnitude but opposite in sign. Therefore, in BB-PD the force density of a bond $\boldsymbol{\xi}$ is called the pairwise force function **f**. These assumptions simplify the formulation; however, BB-PD is restricted to a fixed value of Poisson's ratio which is $\nu = 1/4$ for 3D and plane strain cases and $\nu = 1/3$ for plane stress cases. Ref. [7] introduces the Prototype Microelastic Brittle (PMB) model for a linear elastic material so that the pairwise force function, for the case of small deformation, is determined by:

$$\boldsymbol{f}(\boldsymbol{u}'-\boldsymbol{u},\boldsymbol{x}'-\boldsymbol{x},t) = \mu(\xi,t)\frac{c\omega(\xi)}{|\xi|}\big(\boldsymbol{u}(x')-\boldsymbol{u}(x)\big)\boldsymbol{e} = \mu(\xi,t)c(|\xi|)\big(\boldsymbol{u}(x')-\boldsymbol{u}(x)\big)\boldsymbol{e} \qquad (3)$$

where μ is a history dependent damage function that, based on the bond status, takes either the value of 0 (broken bond) or 1 (active bond). $c(|\xi|)$ is the micromodulus function, c is the micromodulus, ω is the influence function that specifies the degree of nonlocal interactions between points, $\boldsymbol{e}$ is the unit vector along the directions of the relative position vector in the current configuration; c can be expressed in terms of material classical constants E and ν [1,8]. In the PMB material the failure of a bond happens when the relative elongation of a bond exceeds a predefined value s_0 the value of which can be obtained in terms of the critical energy release rate of the material G_0 [7,9]. In the present paper, we make use of a meshfree discretization scheme introduced in [7] which is easy to implement. Each node $\mathbf{x}_i$ interacts with all nodes within its neighbourhood $H(\mathbf{x}_i)$, $\mathbf{x}_i$ is the source node and all $\mathbf{x}_j$ are its family nodes. The horizon δ is expressed as $\delta = m\,\Delta x$. m is the ratio between the horizon δ and the grid spacing

Δx and its value determines how many family nodes are in $H(\mathbf{x}_i)$. To proceed with the spatial integration, we adopt the one-point Gauss quadrature rule and thus the discretized form of Eq.(1) can be written as:

$$\rho\ddot{\boldsymbol{u}}_i^n = \begin{cases} \sum_j \{\underline{\boldsymbol{T}}[\boldsymbol{x}_i^n]\langle \boldsymbol{x}_j^n - \boldsymbol{x}_i^n\rangle - \underline{\boldsymbol{T}}[\boldsymbol{x}_j^n]\langle \boldsymbol{x}_i^n - \boldsymbol{x}_j^n\rangle\}\beta(\boldsymbol{\xi})\boldsymbol{V}_j + \boldsymbol{b}_i^n, & for\ OSB-PD \\ \sum_j \boldsymbol{f}(\boldsymbol{u}_j^n - \boldsymbol{u}_i^n, \boldsymbol{x}_j - \boldsymbol{x}_i)\,\beta(\boldsymbol{\xi})\boldsymbol{V}_j + \boldsymbol{b}_i^n, & for\ BB-PD \end{cases}, \forall \boldsymbol{x}_j \in H(\boldsymbol{x}_i) \quad (4)$$

where n represents the time step, and subscripts denote the node number (e.g., $\mathbf{u}^n{}_j = \mathbf{u}(\mathbf{x}_j, t_n)$). $\beta(\xi)$ plays the role of a correction factor through which we can evaluate the portion of V_j that falls within the neighbourhood of the source node $\mathbf{x}_i$. In this study, we apply $\beta(\xi)$ as recommended in [10].

2.2 FEM-PD coupling method

The coupling of PD grids to FEM meshes could be a way to obtain an efficient numerical approach able to combine the capabilities of both FEM and PD methods. The coupling approach is based on the idea presented in [3], where the coupled stiffness matrix is defined.

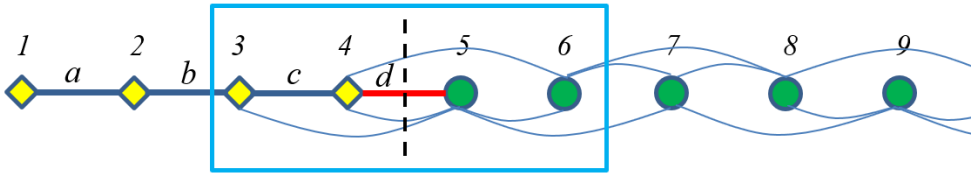

Figure 1: Coupled 1D model of a bar. Diamonds are FEM nodes, circles PD nodes; thick straight lines represent finite elements and thin curved lines peridynamic bonds. The dashed line is the transition between the FEM and the PD portion of the model. The rectangle contains the nodes of the coupling zone.

The coupling method is presented with the help of the simple 1D example of Fig. 1, where a model of a bar is shown. In Fig.1 diamonds represent finite element nodes and circles peridynamic nodes. In the present work, the PD part of the body is discretised in space, according to the bond-based version of the theory. In the example of Fig. 1, the horizon δ is double the grid spacing, i.e. $\delta=2\Delta x$, where Δx is the uniform distance between two adjacent nodes. FEM nodes are connected by finite elements whereas peridynamic nodes are connected by bonds. At the transition between the two zones we assume that the last FEM node (node *4* in Fig.1) is connected to the peridynamic part of the model by a single finite element (element *d* in the figure) whereas the first peridynamic node (node *5* in the figure) is non-locally connected to all nodes, FEM or PD, within its horizon. The coupling zone can be defined where forces are exchanged between the FEM and PD parts of the domain. In the example presented in Fig. 1, the coupling zone is composed of the nodes *3*, *4*, *5*, and *6*. Bonds are considered to act only on PD nodes, whereas finite elements apply forces only on FEM nodes. The assembly of the global stiffness matrix is performed by making sure that equilibrium equations of FEM nodes contain only terms coming from the FEM formulation and equilibrium equations of PD nodes include only terms derived from the Peridynamic theory. The case of Fig.1 produces Eq. (5), where $a=EA/\Delta x$, and $b= cV_iV_j/\Delta x$ [11], u_i are the nodal displacements, f_i are the nodal forces, E is the elastic modulus, A is the cross-sectional area, $c=2EA/\delta^2$ is the micromodulus constant [11], and V_i is the volume associated with node i. The solution of a single equation satisfies node equilibrium. The overall equilibrium of the whole structure requires the sum of the nodal forces to be equal to zero.

$$\begin{bmatrix} a & -a & 0 & 0 & 0 & 0 & 0 & 0 & 0 & 0 \\ -a & 2a & -a & 0 & 0 & 0 & 0 & 0 & 0 & 0 \\ 0 & -a & 2a & -a & 0 & 0 & 0 & 0 & 0 & 0 \\ 0 & 0 & -a & 2a & -a & 0 & 0 & 0 & 0 & 0 \\ 0 & 0 & -\frac{b}{4} & -b & 2.5b & -b & -\frac{b}{4} & 0 & 0 & 0 \\ 0 & 0 & 0 & -\frac{b}{4} & -b & 2.5b & -b & -\frac{b}{4} & 0 & \vdots \\ 0 & 0 & 0 & 0 & -\frac{b}{4} & -b & 2.5b & -b & -\frac{b}{4} & \vdots \\ 0 & 0 & 0 & 0 & \cdots & \cdots & \cdots & \ddots & \vdots & \vdots \\ 0 & 0 & 0 & 0 & \cdots & \cdots & \cdots & \cdots & \ddots & \vdots \end{bmatrix} \begin{bmatrix} u_1 \\ u_2 \\ u_3 \\ u_4 \\ u_5 \\ \vdots \\ \vdots \\ \vdots \\ \vdots \\ u_N \end{bmatrix} = \begin{bmatrix} f_1 \\ f_2 \\ f_3 \\ f_4 \\ f_5 \\ \vdots \\ \vdots \\ \vdots \\ \vdots \\ f_N \end{bmatrix} \tag{5}$$

3 OUT OF BALANCE FORCES IN OVERALL EQUILIBRIUM

3.1 Problem description

In Fig. 2, the 2D model of a homogeneous, isotropic and linear elastic rectangular plate is shown. This structure with dimensions 80x40 (L_x and L_y, respectively) is studied imposing as a load condition two vertical forces (F_{ext}= *-0.5*) acting at the top edge. The plate is constrained so that the points of the bottom edge of coordinates (*x=10*) and (*x=70*) cannot move along the vertical direction, i.e. *v*=0. The central point of the bottom edge cannot move along the horizontal direction, i.e. *u*=0. The values of the main model parameters are *E=1* (Young's modulus), ν= 1/3 (Poisson's ratio) and *h*=1 (plate thickness). Model parameters such as *E, A, Lx, Ly, Δx=Δy* are given conventional values which are not associated to the usual units. This study considers a plane stress condition. To investigate the static equilibrium of this structure, three models have been implemented using three different computational approaches, i.e. Finite Element method, bond-based Peridynamic theory (BBPD) and the FEM-PD coupling strategy described in Sec 2.2.

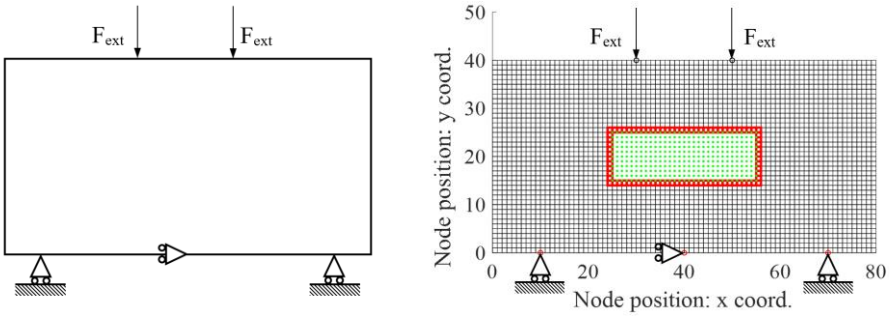

Figure 2: On the left the studied 2D model is shown, the boundary conditions are applied on the bottom edge, in the upper edge 2 vertical external forces are applied. On the right the coupled FEM-PD model is shown, the PD region, located at the centre of the plate, is shown using dot markers.

Model description	$\Sigma F_{ext\ vertical}$	$\Sigma R_{vertical}$	e_r
Only FEM	-1.0	1.00000	$2.52 \cdot 10^{-14}$
Only PD	-1.0	1.00000	$4.27 \cdot 10^{-14}$
FEM-PD coupled	-1.0	1.00699	$6.99 \cdot 10^{-03}$

Table 1: Reaction forces and out of balance relative error resulting for each numerical simulation.

Table 1 reports the reaction values for the three models and the resulting out-of-balance relative error, defined by the following relation:

$$e_r = \frac{F_{ext} + \sum Reactions}{|F_{ext}|} \tag{6}$$

where Σ*Reactions* is the sum of the vertical reaction forces. Table 1 shows that the static equilibrium equations are not exactly fulfilled by the coupled FEM-PD models characterized by non-uniform strain distributions. The out of balance forces are rather small, compared to the overall forces, but they are not as small as round-off errors. To examine this issue a simpler 1D case is studied in the following section.

4 NUMERICAL EXAMPLES

The proposed coupling method assumes the continuity of the displacements between the two portions of the model, in [3] authors showed that for a linear or quadratic displacement field distribution the force equilibrium is satisfied. In this section the equilibrium check will be extended to more complex displacement fields distributions. The 1D model of a bar is composed by 51 nodes as shown in Fig. 4. The PD portion of the model is composed by nodes with coordinates higher than 0.5 while the remaining part is modelled with FEM. The main parameters are $L=1$ (bar length), $E=1$ (elastic modulus) and $A=1$ (bar cross-sectional area). For the PD region of the model the horizon is δ=0.06, the m ratio is m=3 and the micromodulus c is $c=2EA/\delta^2$=555.555. In the FEM-PD coupled model the displacement is imposed to all nodes and the required nodal forces are computed using Eq.(5). The imposed displacement field is defined by a polynomial curve, with the following equation:

$$u(x) = a_0 \cdot x^{\gamma} \tag{7}$$

in which the coefficient a_0 is $a_0=0.01$ and the exponent γ can vary, in this study, between 1 and 4. The resulting out of balance relative error is evaluated in the X direction through the following relation

$$e_r = \frac{\Sigma f}{(\Sigma f)/2} \tag{8}$$

Where Σf is the sum of the nodal forces generated by the applied displacement field.

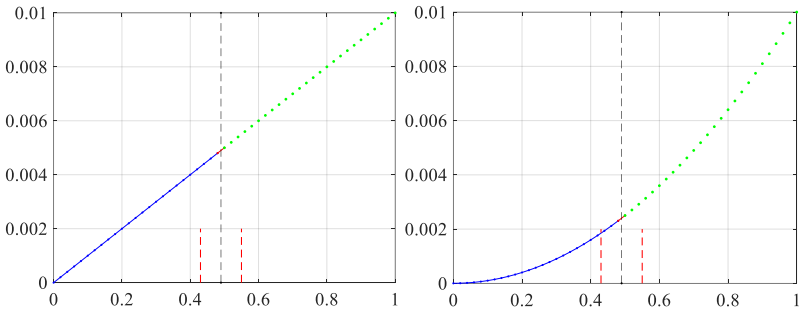

Figure 3: displacement fields imposed on the coupled FEM-PD model; left, linear displacement distribution ($\gamma=1$); right, quadratic displacement distribution ($\gamma=2$). Green dots are PD nodes, short dashed red vertical lines define the coupling zone.

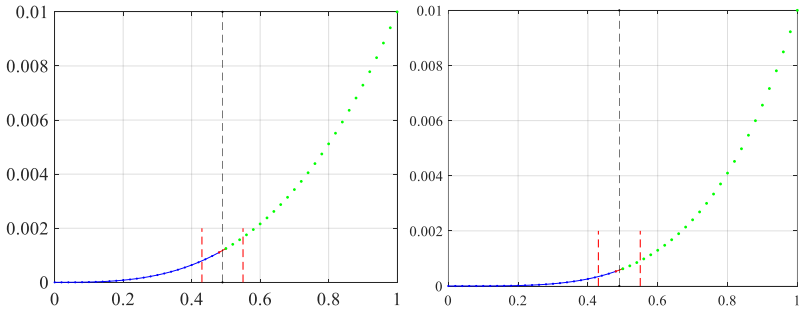

Figure 4: displacement fields imposed on the coupled FEM-PD model; left, displacement distribution described by a third order polynomial function ($\gamma=3$); right, displacement distribution described by a fourth order polynomial function ($\gamma=4$).

Exponent used in Eq. (7)	Σf	e_r	FEM force at the transition	PD force flux at the transition
$\gamma = 1$ (linear displ. distr.)	$-2.39\cdot10^{-16}$	$-2.39\cdot10^{-14}$	0.010000	0.010000
$\gamma = 2$ (quadratic displ. distr.)	$-2.98\cdot10^{-16}$	$-1.57\cdot10^{-14}$	-0.009800	-0.009800
$\gamma = 3$ (third order displ. distr.)	$8.00\cdot10^{-6}$	$2.95\cdot10^{-04}$	0.007204	0.007212
$\gamma = 4$ (fourth order displ. distr.)	$1.57\cdot10^{-5}$	$4.57\cdot10^{-04}$	0.0047079	0.0047236

Table 2: Reaction forces and relative out-of-balance error resulting from each numerical simulation.

The results collected in Table 2 show that the relative out-of-balance error appears when the applied displacement field distribution is described with a polynomial function of the third-order or higher. The table reports also the forces at the transition between the FEM and PD region evaluated respectively with the FEM method and the PD approach (see appendix in [3]). In an equilibrated system these forces should be equal.

In the second example we verify that the lack of the equilibrium in the coupled FEM-PD model occurs only if the highly non-linear rate of change of the applied displacement appears in the coupling zone. In this example the applied displacements field is composed by 2 linear displacement distributions and between them a third-order polynomial curve selected to ensure the continuity of the displacement field and its first derivative. For all cases the magnitude of the relative out-of-balance error, e_r, is computed by keeping fixed the position of the PD portion and all the main model parameters and by changing only the position of the third-order polynomial displacement distribution field.

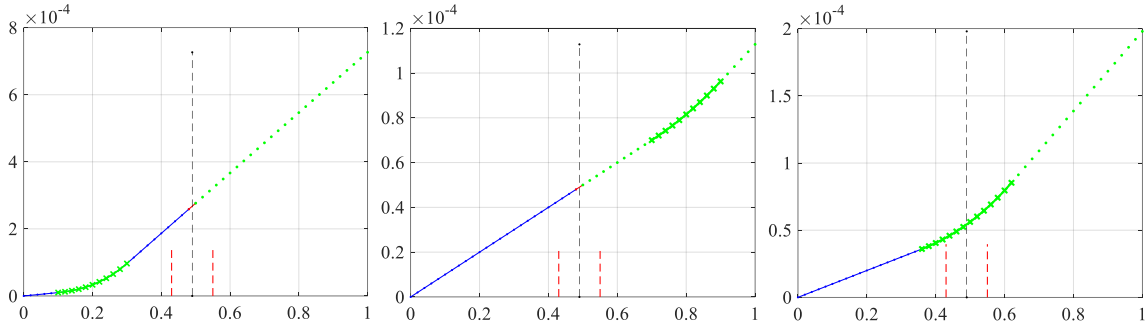

(a) (b) (c)

Figure 5: Imposed displacement fields with a cubic displacement distribution located in different positions along the one-dimensional FEM-PD coupled model. The cubic displacement distribution, represented by crossed lines, is placed in (a) the FEM-only region, (b) the PD-only part, and (c) the FEM-PD coupling zone.

Table 3 shows the results obtained in terms of external reaction forces sum and out-of-balance error for the three different configurations which have been investigated. In the first two cases (see configurations (a), (b) in Fig. 5) the third-order polynomial displacement distribution is located away from the two coupling zones of the bar model, respectively in the FEM-only and in the PD-only portion of the model. In the case (c) the polynomial curve is placed in correspondence of the coupling zone. As shown in Table 3, only case (c) exhibits a significant static out of balance, since the magnitude of the resulting relative error cannot be considered as numerical error. The numerical simulations show that the resulting relative out-of-balance error changes significantly when varying the position of the polynomial displacement distribution with respect to that of the coupling zone.

δ=0.06, m=3	Σ*f*	e_r
Case (a)	$-2.26\cdot10^{-17}$	$-2.51\cdot10^{-14}$
Case (b)	$-3.31\cdot10^{-18}$	$-2.00\cdot10^{-14}$
Case (c)	$2.06\cdot10^{-07}$	$6.94\cdot10^{-04}$

Table 3: Reaction forces and relative out-of-balance error resulting for the cases presented in Fig.5.

The last example investigates the influence of the horizon size δ on the relative out-of-balance error. The horizon δ is reduced by keeping fixed the m ratio, Fig. 6 shows the applied displacement fields for the first three cases studied and Tab.4 reports the relevant relative out-of-balance errors.

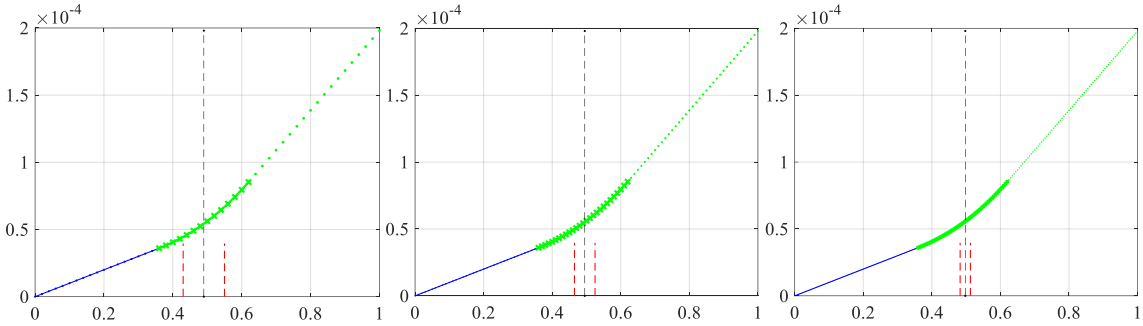

Figure 6: Imposed displacement fields with the cubic displacement distribution, represented by crossed lines, located across the FEM-PD coupling zone (Case (c) in Fig.5). The plots have been obtained by keeping fixed the position of the cubic curve and performing a δ-convergence study.

PD model parameters	Σ*f*	e_r
δ=0.06, m=3	$2.06\cdot10^{-07}$	$6.94\cdot10^{-04}$
δ=0.03, m=3	$5.14\cdot10^{-08}$	$1.73\cdot10^{-04}$
δ=0.015, m=3	$1.29\cdot10^{-08}$	$4.34\cdot10^{-05}$
δ=0.0075, m=3	$3.22\cdot10^{-09}$	$1.08\cdot10^{-05}$

Table 4: Reaction forces and relative out-of-balance error obtained locating the cubic curve across the FEM-PD coupling zone (see Case (c) in Fig.5) and performing a δ-convergence study.

Tab.4 shows that the relative out-of-balance error can be reduced by decreasing the horizon size. Finally, Fig.7 verifies that the relation between the relative out-of-balance error and the quantity δ^2 is linear: if the horizon δ is reduced by ½ the relative out-of-balance error is decreased by a factor ¼.

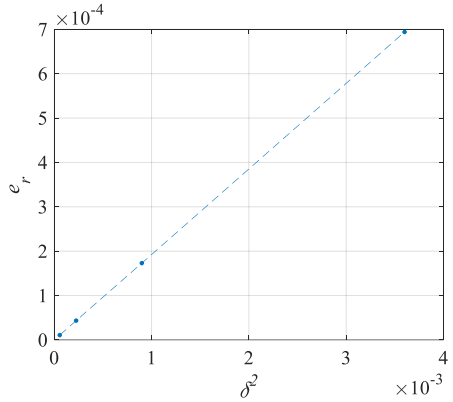

Figure 7: Variation of the relative out-of-balance error versus δ^2. The dashed line is the linear fitting curve.

5 CONCLUSIONS

Coupling different models of solid mechanics to describe the mechanical behaviour of a body can produce some kind of error. The paper focuses on a peridynamic and FEM coupling

computational method proposed by the authors [3], but probably similar problems can affect other coupling techniques. We show, for the first time, that an often-overlooked issue in the use of coupled models is the lack of overall equilibrium. We study the problem through a set of numerical analyses on one-dimensional and two-dimensional FEM-PD coupled models. We show that the out-of-balance forces are related to the rate of change of displacements in the coupling zone: the issue appears for cubic, or higher order, displacement field distributions. The relative out-of-balance error is a fraction of a per cent and it can be controlled by reducing the horizon size. This suggests that a generic rapidly varying strain distribution could require a fine mesh/grid in the coupling zone, where the real strain distribution could be represented, with acceptable accuracy, as a linearly varying strain.

6 ACKNOWLEDGEMENTS

The authors would like to acknowledge the support they received from University of Padua under the research project BIRD2017 NR.175705/17 and BIRD2018 NR.183703/18, the National Key Research and Development Program of China (2017YFC1501102) and the Chinese Scholarship Council (No. 201706710018).

REFERENCES

[1] S. Silling. Reformulation of elasticity theory for discontinuities and long-range forces. *J. Mech. Phys. Solids*, **48**, pp.175-209 (2000).
[2] S. Silling, R. Leouchq. Peridynamic theory of solid mechanics. *Adv. Appl. Mech*., **44**, pp. 73-168, (2010).
[3] M. Zaccariotto, T. Mudric, D. Tomasi, A. Shojaei, U. Galvanetto. Coupling of FEM meshes with Peridynamic grids. *Comp. Meth. Appl. Mech. Eng.*, **330**, pp. 471-497, (2018).
[4] P. Diehl, S. Prudhomme, M. Lévesque. A review of benchmark experiments for the validation of peridynamics models. *J. Peridynamics and Nonlocal Mod.*, pp. 1-22, (2019).
[5] Le Q., Chan W., Schwartz J.; A two-dimensional ordinary, state-based peridynamic model for linearly elastic solids. *Int J Numer Methods Eng*, **98(8)**, pp.547-61, (2014).
[6] Sarego G, Le QV, Bobaru F, Zaccariotto M, Galvanetto U. Linearized state-based peridynamics for 2-D problems. *Int J Numer Methods Eng*, **108(10)**, pp.1174–97, (2016).
[7] Silling S, Askari E. A meshfree method based on the peridynamic model of solid mechanics. *Comput Struct*, **83(17–18)**, pp. 1526–35, (2005).
[8] F. Bobaru, J. T. Foster, P. H. Geubelle, and S. A. Silling. Handbook of peridynamic modeling. CRC press, New York, (2016).
[9] Ha YD, Bobaru F. Studies of dynamic crack propagation and crack branching with peridynamics. *Int J Fract*, **162(1–2)**, pp. 229–44, (2010).
[10] P. Seleson. Improved one-point quadrature algorithms for two-dimensional peridynamic models based on analytical calculations. *Comput. Methods Appl. Mech. Engrg*., **282**, pp.184–217, (2014).
[11] F. Bobaru, M. Yang, L. F. Alves, S. A. Silling, E. Askari, J. Xu, Convergence, adaptive refinement, and scaling in 1d peridynamics, *Int J Num Meth Eng*, **77(6)**, pp. 852–877, (2009).